Tetrahedron 69 (2013) 1965–1969

Contents lists available at SciVerse ScienceDirect

Tetrahedron

journal homepage: www.elsevier.com/locate/tet

Highly selective fluorescent sensors for mercury(II) ions and their applications in living cell imaging

Hsuan-Fu Wang, Shu-Pao Wu *

Department of Applied Chemistry, National Chiao Tung University, Hsinchu 300, Taiwan, ROC

ARTICLE INFO

Article history:
Received 19 November 2012
Received in revised form 24 December 2012
Accepted 31 December 2012
Available online 8 January 2013

Keywords:
Sensors
Mercury(II)
Pyrene
Imaging agents

ABSTRACT

Three new pyrene derivatives (**MS1**, **MS2**, and **MS3**) containing two triazole units exhibited fluorescence quenching in the presence of Hg^{2+} ions. Other metal ions Ag^{+}, Ca^{2+}, Cd^{2+}, Co^{2+}, Cu^{2+}, Fe^{2+}, Fe^{3+}, K^{+}, Mg^{2+}, Mn^{2+}, Na^{+}, Ni^{2+}, Pb^{2+}, Rb^{+}, and Zn^{2+} produced only minor changes in the fluorescence of **MS1**, **MS2**, and **MS3**. The binding ratio of the chemosensor-Hg^{2+} complexes was found to be 1:1 according to Job plot experiments. The association constants (K_a) of chemosensor-Hg^{2+} complexes were found to be 1.68×10^3 M^{-1} (**MS1**), 1.57×10^3 M^{-1} (**MS2**), and 1.52×10^3 M^{-1} (**MS3**), respectively. Moreover, fluorescence microscopy experiments showed that **MS1** could be used as a fluorescent probe for detecting Hg^{2+} in living cells.

1. Introduction

The development of fluorescent chemosensors for the detection of metal ions such as Cu^{2+}, Cd^{2+}, Fe^{3+}, Hg^{2+}, Pb^{2+}, and Zn^{2+}, has been an important topic.[1] Mercury is one of the most hazardous species and shows a high affinity for thiol groups in proteins.[2] This leads to the malfunction of cells and consequently causes much damage to the brain, kidney, and central nervous system. Its accumulation in the human body causes prenatal brain damage, serious cognitive and motive disorders, vision and hearing loss, and even death.[3] Due to its high toxicity, the United States Environmental Protection Agency (EPA) established the standard maximum allowable level of mercury in dietary and environmental sources to be 2 ppb (10 nM).

Determination of Hg^{2+} in various samples has been an important issue in the area of environmental protection and food safety. Several methods[4] for mercury detection have been developed, including atomic absorption/emission spectroscopy,[5] inductively coupled plasma-mass spectroscopy (ICPMS),[6] inductively coupled plasma-atomic emission spectrometry (ICP-AES),[7] and voltammetry.[8] Most of these methods require expensive instruments and are not suitable for onsite assays. Recently, more attention has been focused on the development of fluorescent chemosensors for the detection of Hg^{2+} ions.[9]

In this study, three pyrene-based fluorescent chemosensors were designed for metal ion detection. Two parts make up the chemosensors: a pyrene moiety as a reporter, and a triazole-ether unit as a chelator for the metal ion (Scheme 1). Chemosensors **MS1**, **MS2**, and **MS3** exhibit strong fluorescence due to the formation of pyrene excimer. Binding metal ions to the chemosensor forbids the formation of pyrene excimer and also results in fluorescence quenching. The metal ions Ag^{+}, Ca^{2+}, Cd^{2+}, Co^{2+}, Cu^{2+}, Fe^{2+}, Fe^{3+}, Hg^{2+}, K^{+}, Mg^{2+}, Mn^{2+}, Na^{+}, Ni^{2+}, Pb^{2+}, Rb^{+}, and Zn^{2+} were tested for metal ion binding selectivity with chemosensors, but Hg^{2+} was the only ion that caused an obvious fluorescence quenching upon binding with chemosensors **MS1**, **MS2**, and **MS3**.

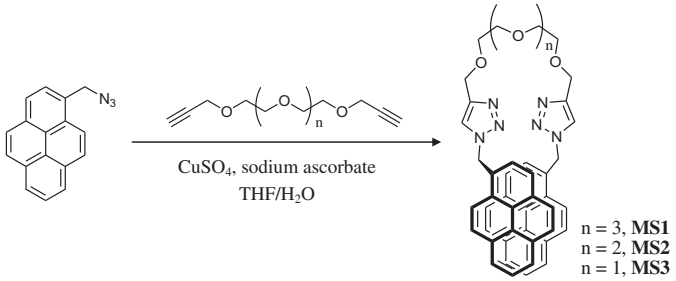

Scheme 1. Synthesis of **MS1**, **MS2**, and **MS3**.

2. Results and discussion

2.1. Synthesis of MS1, MS2, and MS3

Chemosensors **MS1**, **MS2**, and **MS3** were synthesized through the click reaction of 1-(azidomethyl)pyrene with corresponding

* Corresponding author. Tel.: +886 3 5712121x56506; fax: +886 3 5723764; e-mail addresses: spwu@mail.nctu.edu.tw, spwu@faculty.nctu.edu.tw (S.-P. Wu).

0040-4020/$ – see front matter © 2013 Elsevier Ltd. All rights reserved.
http://dx.doi.org/10.1016/j.tet.2012.12.075

polyoxyethylene dialkyne to form a triazole structure between ether and pyrene (Scheme 1). Chemosensors **MS1**, **MS2**, and **MS3** are colorless and have an absorption band centered at 343 nm, which is an 8-nm red shift from the typical absorption band of pyrene, 335 nm.[10] Compared to the structure of pyrene, chemosensors **MS1**, **MS2**, and **MS3** do not have longer conjugated double bonds, which account for similar UV–vis absorption wavelength of chemosensors **MS1**, **MS2**, and **MS3** compared to pyrene. In addition, chemosensors **MS1**, **MS2**, and **MS3** exhibit a strong excimer emission at 474 nm and a weak monomer emission at 378 nm.

2.2. Cation-sensing properties

The sensing abilities of chemosensor **MS1**, **MS2**, and **MS3** were tested by mixing them with the metal ions Ag^{+}, Ca^{2+}, Cd^{2+}, Co^{2+}, Cu^{2+}, Fe^{2+}, Fe^{3+}, Hg^{2+}, K^{+}, Mg^{2+}, Mn^{2+}, Na^{+}, Ni^{2+}, Pb^{2+}, Rb^{+}, and Zn^{2+}. In Fig. 1, Hg^{2+} was the only ion that caused a fluorescence quenching from chemosensor **MS1**. Chemosensors **MS2** and **MS3** show similar results. During Hg^{2+} titration with chemosensor **MS1**, the absorbance at 343 nm did not change (Fig. 2). This indicates that Hg^{2+} binding with chemosensor **MS1** did not affect any absorption properties of the chemosensor. For the fluorescence spectra of chemosensor **MS1**, an emission band centered at 474 nm decreased during Hg^{2+} titration with chemosensor **MS1** (Fig. 2). After adding 1.0 equiv of Hg^{2+}, the emission intensity reached a minimum. The quantum yield of the **MS1**–Hg^{2+} complex was 0.009, which is 18-fold lower than that of chemosensor **MS1**, 0.16. These observations indicate that Hg^{2+} is the only metal ion that readily binds with chemosensor **MS1**, causing significant fluorescence quenching and permitting highly selective detection of Hg^{2+}.

To study the influence of other metal ions on Hg^{2+} binding with chemosensor **MS1**, competitive experiments were performed with other metal ions (25.0 μM) in the presence of Hg^{2+} (25.0 μM) (Fig. 3). Fluorescence quenching caused by the mixture of Hg^{2+} with most metal ions was similar to that caused by Hg^{2+} alone. Smaller fluorescence quenching was observed only when Hg^{2+} was mixed with Na^{+}, Rb^{+} or K^{+}, indicating that Na^{+}, Rb^{+}, and K^{+} compete with Hg^{2+} for binding with chemosensor **MS1**. None of the other metal ions were found to interfere with the binding of chemosensor **MS1** with Hg^{2+}. Chemosensor **MS2** had similar results, but **MS3** did not (see Fig. S7 in Supplementary data). In the presence of most other metal ions, smaller fluorescence quenching of **MS3** was observed. This indicates that Hg^{2+} binding with chemosensor **MS3** is influenced by other metal ions.

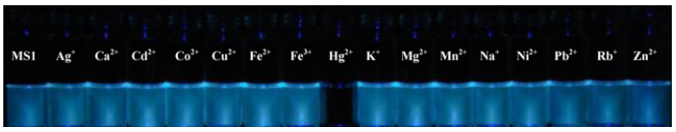

Fig. 1. Fluorescence change of **MS1** (100 μM) with 200 μM of metal ions in acetonitrile/water (v/v=4:1) solutions.

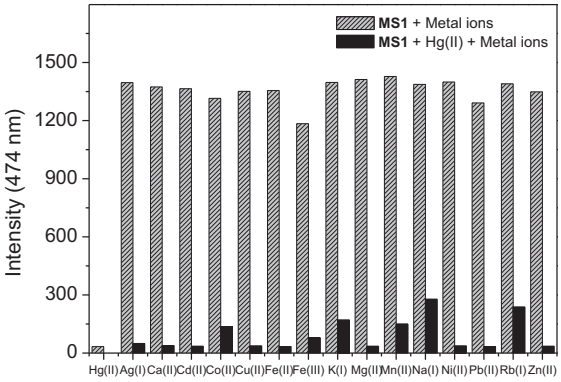

Fig. 3. Fluorescence response of chemosensor **MS1** (25 μM) to the addition of Hg^{2+} (25 μM) or 25 μM of other metal ions (gray bars) and to the mixture of other metal ions (25 μM) with 25 μM of Hg^{2+} (black bars) in acetonitrile/water (v/v=4:1) solutions. The excitation wavelength is 343 nm.

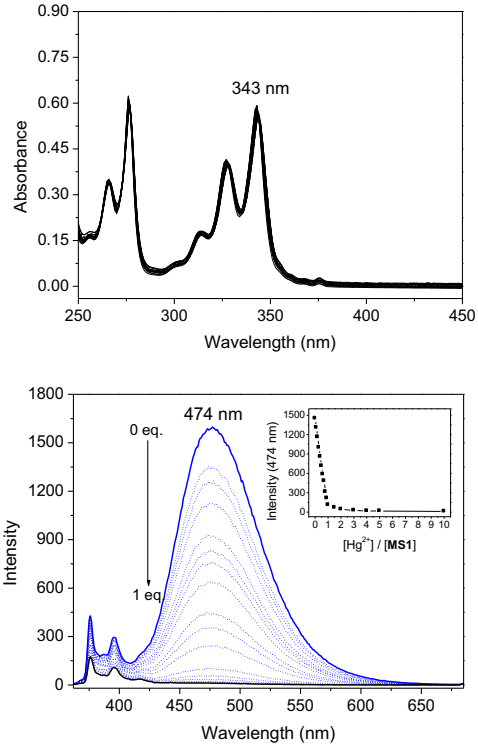

Fig. 2. Absorption (top) and fluorescence (bottom) response of chemosensor **MS1** (25 μM) to various equivalents of Hg^{2+} in acetonitrile/water (v/v=4:1) solutions. The excitation wavelength was 343 nm.

In order to understand the binding stoichiometry of **MS1**–Hg^{2+} complexes, Job plot experiments were carried out. In Fig. 4, the emission intensity at 474 nm is plotted against molar fraction of chemosensor **MS1** under a constant total concentration (20 μM). Minimum emission intensity was reached when the molar fraction was 0.5. This result indicates a 1:1 ratio for **MS1**–Hg^{2+} complexes, in which one Hg^{2+} ion was bound with one chemosensor **MS1**. The formation of a 1:1 **MS1**–Hg^{2+} complex was confirmed by ESI-MS, in which the peak at m/z=986.6 indicates a 1:1 stoichiometry for the

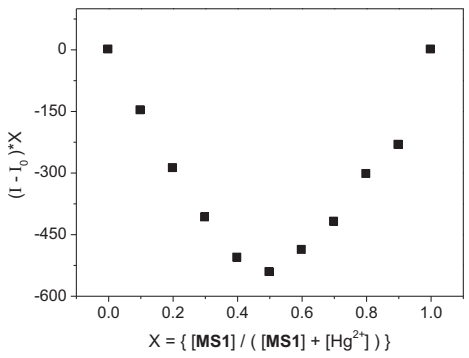

Fig. 4. Job plot of **MS1**-Hg^{2+} complexes in acetonitrile/water (v/v=4:1) solutions. The total concentration of **MS1** and Hg^{2+} was 20.0 μM. The monitored wavelength was 474 nm.

MS1–Hg^{2+} complex (see Fig. S10 in Supplementary data). The association constant K_a was evaluated graphically by plotting $1/\Delta F$ against $1/[Hg^{2+}]$ (Fig. 5). The data were linearly fit and the K_a value was obtained from the slope and intercept of the line. The association constants (K_a) of Hg^{2+} binding in chemosensors **MS1**, **MS2**, and **MS3** were found to be 1.68×10^3 M^{-1} (**MS1**), 1.57×10^3 M^{-1} (**MS2**), and 1.52×10^3 M^{-1} (**MS3**). The detection limits of chemosensors **MS1**, **MS2**, and **MS3** as a fluorescent sensor for the analysis of Hg^{2+} were determined from the plot of fluorescence intensity as a function of the concentration of Hg^{2+} (see Figs. S13–S15 in Supplementary data). It was found that chemosensors **MS1**, **MS2**, and **MS3** have a detection limit of 1.74 μM (**MS1**), 2.42 μM (**MS2**), and 3.83 μM (**MS3**), respectively, which allows the detection of the micromolar concentration range of Hg^{2+}.

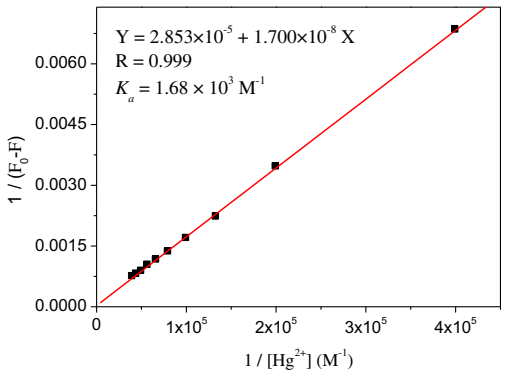

Fig. 5. Benesi–Hildebrand plot of the Hg^{2+}–**MS1** complexes in acetonitrile/water (v/v=4:1) solution. The excitation wavelength was 343 nm and observed wavelength was 474 nm.

To gain a clearer understanding of the structure of the **MS1**–Hg^{2+} complex, ^1H NMR spectroscopy (Fig. 6) was employed. Hg^{2+} is a heavy metal ion and can affect the proton signals that are close to the Hg^{2+} binding site.[11] The ^1H NMR spectra of **MS1** recorded with increasing amounts of Hg^{2+} show that the proton (H_f, triazole) signal at δ=7.65 ppm was shifted downfield as Hg^{2+} was added. This indicates that Hg^{2+} binds to **MS1** mainly through the nitrogen atom in the triazole ring. The proton signal (H_e) shifted upfield upon addition of Hg^{2+}. This also indicates that Hg^{2+} binds through the ether structure attached to the triazole ring. The proton signals (H_a and H_b) also shifted upfield upon addition of Hg^{2+}. Because Hg^{2+} binding to **MS1** caused the separation of two pyrenes, this resulted in an upfield shift of the proton signals (H_a and H_b). These observations show that Hg^{2+} binds to **MS1** through two triazole nitrogen atoms and two ether oxygen atoms.

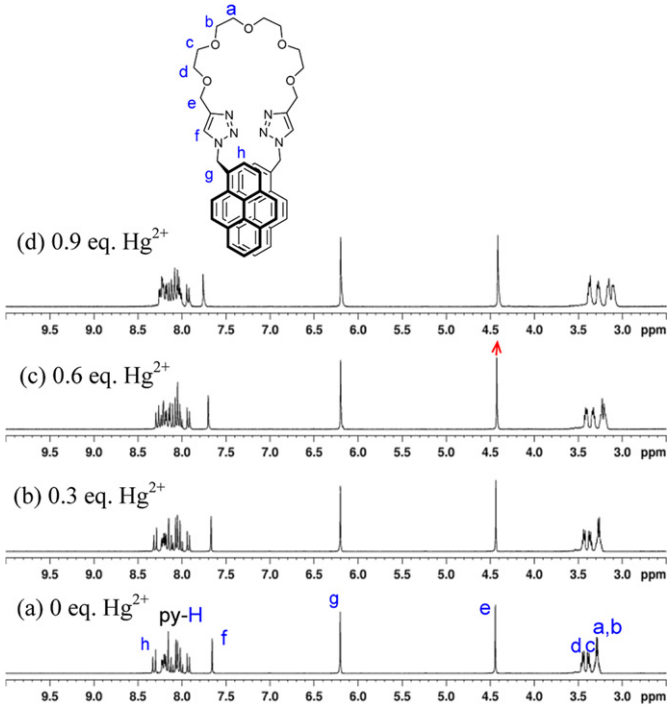

Fig. 6. ^1H NMR spectra of **MS1** (25 mM) in the presence of Hg^{2+} in CD_3CN.

To investigate the structures of **MS1** and **MS1**–Hg^{2+} complexes, density functional theory (DFT) calculations were employed by using the Gaussian 09 package. Chemosensor **MS1** and **MS1**–Hg^{2+} complexes were subjected to energy optimization by using B3LYP/6-31G and B3LYP/LANL2DZ, respectively. The global minima structures for **MS1** and **MS1**–Hg^{2+} complexes are shown in Fig. 7. For **MS1**, one pyrene faces the other pyrene to form a Py–Py* excimer, which contributes to the emission at 474 nm. For **MS1**–Hg^{2+} complex, Hg^{2+} binds to **MS1** through two nitrogen atoms (2.59, 2.60 Å) and two oxygen atoms (2.95, 2.97 Å), respectively (see Fig. S16 in Supplementary data). Hg^{2+} binding to **MS1** causes the separation of two pyrenes by about 11.7 Å, resulting in a decrease of the Py–Py* excimer emission and also causing fluorescence quenching.

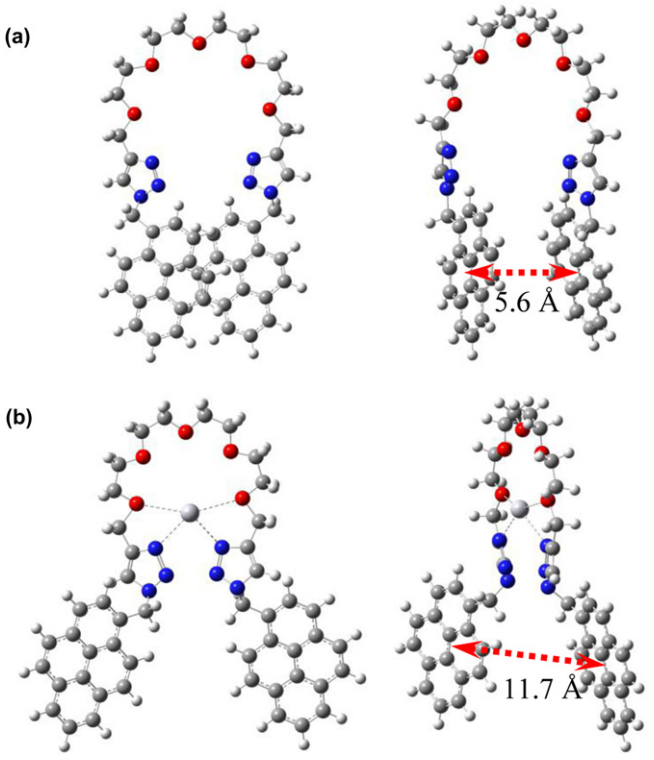

Fig. 7. DFT-optimized structures of **MS1** (top) and **MS1**–Hg^{2+} complexes (bottom). Red atom, O; blue atom, N; gray atom, Hg.

2.3. Living cell imaging

Chemosensor **MS1** was used for living cell imaging. To detect Hg^{2+} in living cells, RAW 264.7 cells were cultured in DMEM supplemented with 10% FBS at 37 °C and 5% CO_2. Cells were plated on 18 mm glass coverslips and allowed to adhere for 24 h. RAW 264.7 cells were treated with 20 μM $Hg(BF_4)_2$ for 30 min and washed with PBS three times. The cells were then incubated with chemosensor **MS1** (20 μM) for 30 min and washed with PBS to remove the

remaining sensor. The images of the RAW 264.7 cells were obtained using a fluorescence microscope. Fig. 8 shows the images of RAW 264.7 cells with chemosensor **MS1** after treatment of Hg^{2+}. An overlay of fluorescence and bright-field images shows that the fluorescence signals are localized in the intracellular area, indicating a subcellular distribution of Hg^{2+} and good cell-membrane permeability of chemosensor **MS1**.

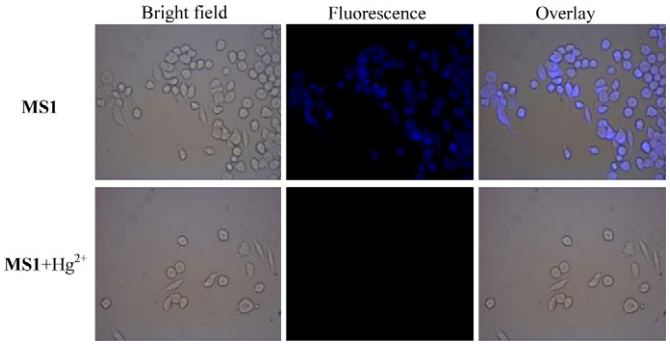

Fig. 8. Fluorescence images of RAW 264.7 macrophage treated with **MS1** and Hg^{2+}. (Left) bright-field image; (middle) fluorescence image; and (right) merged image.

3. Conclusion

In summary, we presented three pyrene-based fluorescent chemosensors for Hg^{2+} sensing. Three chemosensors **MS1**, **MS2**, and **MS3** were synthesized from the click reaction of 1-(azidomethyl)pyrene and polyoxyethylene dialkyne to form a triazole ring between ether structure and pyrene. We observed significant fluorescence quenching with chemosensors **MS1**, **MS2**, and **MS3** in the presence of Hg^{2+}. However, adding Ag^{+}, Ca^{2+}, Cd^{2+}, Co^{2+}, Cu^{2+}, Fe^{2+}, Fe^{3+}, K^{+}, Mg^{2+}, Mn^{2+}, Na^{+}, Ni^{2+}, Pb^{2+}, Rb^{+} or Zn^{2+} to the chemosensor solution caused only a minimal change in fluorescence emission. In addition, chemosensor **MS1** can be applied in fluorescence imaging of living cells. This pyrene-based Hg^{2+} chemosensor provides an effective probe for Hg^{2+} sensing.

4. Experiment section

4.1. Materials and instrumentations

All solvents and reagents were obtained from commercial sources and used as received without further purification. UV/vis spectra were recorded on an Agilent 8453 UV/Vis spectrometer. IR data were obtained on Bomem DA8.3 Fourier-Transform Infrared Spectrometer. NMR spectra were obtained on Bruker DRX-300 NMR and Varian Unity INOVA-500 NMR spectrometer.

4.2. General procedures for the synthesis of MS1, MS2, and MS3

$CuSO_4 \cdot 5H_2O$ (25 mg, 0.1 mmol) and sodium ascorbate (40 mg, 0.2 mmol) were dissolved in 5 mL of H_2O, and then added into 4,7,10,13,16-pentaoxanonadeca-1,18-diyne[12] (135 mg, 0.5 mmol), 4,7,10,13-tetraoxahexadeca-1,15-diyne[12] (113 mg, 0.5 mmol), and 4,7,10-trioxatrideca-1,12-diyne[12] (92 mg, 0.5 mmol) in THF (10 mL), respectively. 1-(Azidomethyl)pyrene[13] (283 mg, 1.1 mmol) was added into the reaction mixture and the heterogeneous mixture was stirred for 3 days at 50 °C under nitrogen atmosphere. The reaction mixture was extracted three times with dichloromethane (50 mL) and all the organic layers were combined, dried over $MgSO_4$, and then evaporated to give the crude products. The crude products were purified by column chromatography to give yellow viscous compounds **MS1**, **MS2**, and **MS3** in 76%, 73%, and 81% yields, respectively.

*4.2.1. The synthesis of **MS1**.* The crude product was eluted with ethyl acetate/hexane (v/v, 3:1) to give a yellow viscous compound **MS1**. Yield: 76%, 298 mg. ^{1}H NMR (300 MHz, CD_3CN) δ 8.32 (d, J=9.3 Hz, 2H), 8.23–8.02 (m, 14H), 7.93 (d, J=8.1 Hz, 2H), 7.66 (s, 2H), 6.20 (s, 4H), 4.44 (s, 4H), 3.44 (t, J=2.1 Hz, 4H), 3.39 (t, J=2.1 Hz, 4H), 3.31–3.28 (m, 8H); ^{13}C NMR (125 MHz, CD_3CN) δ 146.6, 133.2, 132.7, 132.1, 130.4, 130.0, 129.9, 129.4, 129.2, 128.8, 127.9, 127.3, 127.2, 126.6, 126.1, 125.7, 124.9, 123.9, 70.9, 70.1, 65.3, 53.1, 31.3, 30.3; FTIR (cm^{-1}) 3131, 3042, 2865, 1925, 1768, 1604, 1457, 1348, 1220, 1095, 1047, 847, 707; MS (FAB) found 785.6 $[M+H]^+$; HRMS (FAB) calcd for $C_{48}H_{44}N_6O_5$ 784.3373; found 784.3379.

*4.2.2. The synthesis of **MS2**.* The crude product was eluted with ethyl acetate/hexane (v/v, 3:1) to give a yellow viscous compound **MS2**. Yield: 73%, 270 mg. ^{1}H NMR (300 MHz, CD_3CN) δ 8.26 (d, J=9.0 Hz, 2H), 8.18–7.95 (m, 14H), 7.87 (d, J=7.8 Hz, 2H), 7.62 (s, 2H), 6.14 (s, 4H), 4.39 (s, 4H), 3.39 (t, J=2.1 Hz, 4H), 3.33 (t, J=2.1 Hz, 4H), 3.25 (s, 4H); ^{13}C NMR (125 MHz, CD_3CN) δ 146.6, 133.2, 132.7, 132.1, 130.4, 130.0, 129.9, 129.4, 129.2, 128.8, 128.0, 127.3, 127.2, 126.6, 126.1, 125.6, 124.9, 123.9, 71.7, 70.8, 65.3, 53.1, 30.5; FTIR (cm^{-1}) 3134, 3041, 2865, 1926, 1604, 1457, 1349, 1220, 1095, 1047, 847, 708; MS (FAB) found 741.7 $[M+H]^+$; HRMS (FAB) calcd for $C_{46}H_{40}N_6O_4$ 740.3111; found 740.3115.

*4.2.3. The synthesis of **MS3**.* The crude product was eluted with ethyl acetate/hexane (v/v, 3:1) to give a yellow viscous compound **MS3**. Yield: 81%, 282 mg. ^{1}H NMR (300 MHz, CD_3CN) δ 8.25 (d, J=9.6 Hz, 2H), 8.19–7.97 (m, 14H), 7.90 (d, J=7.8 Hz, 2H), 7.61 (s, 2H), 6.13 (s, 4H), 4,37 (s, 4H), 3.39 (t, J=2.1 Hz, 4H), 3.34 (t, J=2.1 Hz, 4H); ^{13}C NMR (125 MHz, CD_3CN) δ 146.6, 133.2, 132.7, 132.0, 130.4, 130.0, 129.9, 129.4, 129.2, 128.8, 127.9, 127.3, 127.2, 126.5, 126.1, 125.7, 124.9, 123.9, 71.5, 70.8, 65.3, 53.0; FTIR (cm^{-1}) 3134, 3042, 2864, 1589, 1457, 1349, 1220, 1094, 1047, 847, 707; MS (FAB) found 697.7 $[M+H]^+$; HRMS (FAB) calcd for $C_{44}H_{36}N_6O_3$ 696.2849; found 696.2855.

4.3. Metal ion binding study by UV/vis and fluorescence spectroscopy

Chemosensor **MS1** (25 μM) was added with different metal ions (25 μM). All spectra were measured in 1.0 mL acetonitrile/water solution (v/v=4:1). The light path length of cuvette was 1.0 cm.

4.4. Determination of the binding stoichiometry and the apparent association constants K_a of Hg(II) binding in chemosensors MS1, MS2, and MS3

The binding stoichiometry of **MS1**–Hg^{2+} complexes was determined by Job plot experiments.[14] The fluorescence intensity at 474 nm was plotted against molar fraction of **MS1** under a constant total concentration (20 μM). The concentration of the complex approached a minimum intensity when the molar fraction was 0.5. These results indicate that chemosensor **MS1** forms a 1:1 complex with Hg^{2+}. The association constants (K_a) of **MS1**–Hg^{2+} complexes was determined by the Benesi–Hildebrand equation (Eq. 1):[15]

$$1/(F-F_0) = 1\Big/\left\{K_a{}^*(F_{max}-F_0)^*\left[Hg^{2+}\right]\right\} + 1/(F_{max}-F_0) \quad (1)$$

where F is the fluorescence intensity at 474 nm at any given Hg^{2+} concentration, F_0 is the fluorescence intensity at 474 nm in the absence of Hg^{2+}, and F_{max} is the maxima fluorescence intensity at 474 nm in the presence of Hg^{2+} in solution. The association

constant K_a was evaluated graphically by plotting $1/(F-F_0)$ against $1/[Hg^{2+}]$. Typical plots ($1/(F-F_0)$ vs $1/[Hg^{2+}]$) are shown in Fig. 5. Data were linearly fitted according to Eq. 1 and the K_a value was obtained from the slope and intercept of the line.

4.5. Cell culture

RAW 264.7 cells were grown in H-DMEM (Dulbecco's Modified Eagle's Medium, high glucose) supplemented with 10% FBS (Fetal Bovine Serum) in an atmosphere of 5% CO_2 and 95% air at 37 °C.

4.6. Fluorescence imaging

Experiments to assess Hg^{2+} uptake were performed in PBS with 20 μM $Hg(ClO_4)_2$. Treat the cells with 2 μL of 10 mM metal ions (final concentration: 20 μM) dissolved in sterilized PBS (pH 7.4) and incubated for 30 min at 37 °C. The treated cells was washed PBS (2 mL×3) to remove remaining metal ions. Culture medium (2 mL) was added to the cell culture, which was treated with a 10 mM solution of chemosensor **MS1** (2 μL; final concentration: 20 μM) dissolved in DMSO. The samples were incubated at 37 °C for 30 min. The culture media was removed, and the treated cells were washed with PBS (2 mL×3) before observation. Fluorescence imaging was performed with a ZEISS Axio Scope A1 Fluorescence Microscope. Cells loaded with **MS1** were excited at 350 nm using a lamp (Hg 50 W). Emission filter was 420 nm.

4.7. Computational methods

Quantum chemical calculations based on density functional theory (DFT) were carried out using a Gaussian 09 program. Ground state geometry optimization of **MS1** was performed using the B3LYP functional and the 6-31G basis set. Ground state geometry optimization of **MS1**–Hg^{2+} complexes was performed using the B3LYP functional and the LANL2DZ basis set.

Acknowledgements

We gratefully acknowledge the financial support of the National Science Council (ROC) and National Chiao Tung University.

Supplementary data

^1H and ^{13}C NMR spectra of chemosensors **MS1**, **MS2**, and **MS3**, Job plot of **MS2** and **MS3**, Benesi–Hildebrand plot of **MS2** and **MS3**, ESI mass spectra of **MS1**–Hg^{2+}, **MS2**–Hg^{2+}, and **MS3**–Hg^{2+}, detection limit for titration of **MS1**–Hg^{2+}, **MS2**–Hg^{2+}, and **MS3**–Hg^{2+}, DFT-optimized structures of **MS1**–Hg^{2+} complexes. Supplementary data associated with this article can be found in the online version, at http://dx.doi.org/10.1016/j.tet.2012.12.075.

References and notes

1. (a) de Silva, A. P.; Gunaratne, H. Q. N.; Gunnlaugsson, T.; Huxley, A. J. M.; McCoy, C. P.; Rademacher, J. T.; Rice, T. E. *Chem. Rev.* **1997**, *97*, 1515–1566; (b) Nolan, E. M.; Lippard, S. J. *Chem. Rev.* **2008**, *108*, 3443–3480; (c) Kaur, N.; Kumar, S. *Tetrahedron* **2011**, *67*, 9233–9264; (d) Dutta, M.; Das, D. *Trends Anal. Chem.* **2012**, *32*, 113–132; (e) Kim, H. N.; Ren, W. X.; Kim, J. S.; Yoon, J. *Chem. Soc. Rev.* **2012**, *41*, 3210–3244.
2. (a) Boening, D. W. *Chemosphere* **2000**, *41*, 1335–1351; (b) Benoit, J. M.; Fitzgerald, W. F.; Damman, A. W. *Environ. Res.* **1998**, *78*, 118–133; (c) Renzoni, A.; Zino, F.; Franchi, E. *Environ. Res.* **1998**, *77*, 68–72; (d) Harris, H. H.; Pickering, I. J.; George, G. N. *Science* **2003**, *301*, 1203.
3. (a) Takeuchi, T.; Morikawa, N.; Matsumoto, H.; Shiraishi, Y. *Acta Neuropathol.* **1962**, *2*, 40–57; (b) Harada, M. *Crit. Rev. Toxicol.* **1995**, *25*, 1–24.
4. Leopold, K.; Foulkes, M.; Worsfold, P. *Anal. Chim. Acta* **2010**, *663*, 127–138.
5. (a) Gao, Y.; De Galan, S.; De Brauwere, A.; Baeyens, W.; Leermakers, M. *Talanta* **2010**, *82*, 1919–1923; (b) da Silva, M. J.; Paim, A. P. S.; Pimentel, M. F.; Cervera, M. L.; de la Guardia, M. *Anal. Chim. Acta* **2010**, *667*, 43–48.
6. (a) Moreno, F.; Garcia-Barrera, T.; Gomez-Ariza, J. L. *Analyst* **2010**, *135*, 2700–2705; (b) Krishna, M. V. B.; Chandrasekaran, K.; Karunasagar, D. *Talanta* **2010**, *81*, 462–472; (c) Cairns, W. R. L.; Ranaldo, M.; Hennebelle, R.; Turetta, C.; Capodaglio, G.; Ferrari, C. F.; Dommergue, A.; Cescon, P.; Barbante, C. *Anal. Chim. Acta* **2008**, *622*, 62–69; (d) Kenduzler, E.; Atesa, M.; Arslan, Z.; McHenry, M.; Tchounwou, P. B. *Talanta* **2012**, *93*, 404–410.
7. Chai, X.; Chang, X.; Hu, Z.; He, Q.; Tu, Z.; Li, Z. *Talanta* **2010**, *82*, 1791–1796.
8. (a) Fu, X.; Chen, X.; Guo, Z.; Xie, C.; Kong, L.; Liu, J.; Huang, X. *Anal. Chim. Acta* **2011**, *685*, 21–28; (b) Wang, F.; Wei, X.; Wang, C.; Zhang, S.; Ye, B. *Talanta* **2010**, *80*, 1198–1204.
9. (a) Yuan, M.; Li, Y.; Li, J.; Li, C.; Liu, X.; Lv, J.; Xu, J.; Liu, H.; Wang, S.; Zhu, D. *Org. Lett.* **2007**, *9*, 2313–2316; (b) Zhu, M.; Yuan, M.; Liu, X.; Xu, J.; Lv, J.; Huang, C.; Liu, H.; Li, Y.; Wang, S.; Zhu, D. *Org. Lett.* **2008**, *10*, 71481–71484; (c) Hung, H.; Cheng, C.; Wang, Y.; Chen, Y.; Chung, W. *Eur. J. Org. Chem.* **2009**, *36*, 6360–6366; (d) Lee, M. H.; Lee, S. W.; Kim, S. H.; Kang, C.; Kim, J. S. *Org. Lett.* **2009**, *11*, 2101–2104; (e) Vaswani, K. G.; Keranen, M. D. *Inorg. Chem.* **2009**, *48*, 5797–5800; (f) Du, J.; Fan, J.; Peng, X.; Sun, P.; Wang, J.; Li, H.; Sun, S. *Org. Lett.* **2010**, *12*, 476–479; (g) Shi, W.; Sun, S.; Li, X.; Ma, H. *Inorg. Chem.* **2010**, *49*, 1206–1210; (h) Atilgan, S.; Ozdemir, T.; Akkaya, E. U. *Org. Lett.* **2010**, *12*, 4792–4795; (i) Bozdemir, O. A.; Guliyev, R.; Buyukcakir, O.; Selcuk, S.; Kolemen, S.; Gulseren, G.; Nalbantoglu, T.; Boyaci, H.; Akkaya, E. U. *J. Am. Chem. Soc.* **2010**, *132*, 8029–8036; (j) Ahamed, B. N.; Ghosh, P. *Dalton Trans.* **2011**, *40*, 12540–12547; (k) Rode, A. B.; Kim, J.; Kim, S.; Gupta, G.; Hong, I. S. *Tetrahedron Lett.* **2012**, *53*, 2571–2574; (l) Kim, D.; Yamamoto, K.; Ahn, K. H. *Tetrahedron* **2012**, *68*, 5279–5282; (m) Li, C.; Xu, F.; Li, Y.; Zhou, K.; Zhou, Y. *Anal. Chim. Acta* **2012**, *717*, 122–126; (n) Ma, X.; Wang, J.; Shan, Q.; Tan, Z.; Wei, G.; Wei, D.; Du, Y. *Org. Lett.* **2012**, *14*, 820–823; (o) Vedamalai, M.; Wu, S. *Org. Biomol. Chem.* **2012**, *10*, 5410–5416; (p) Fan, J.; Chen, C.; Lin, Q.; Fu, N. *Sens. Actuators, B* **2012**, *173*, 874–881.
10. Maeda, H.; Inoue, Y.; Ishida, H.; Mizuno, K. *Chem. Lett.* **2001**, 1224–1225.
11. Kaupp, M.; Malkina, O. L.; Malkin, V. G.; Pyykko, P. *Chem.—Eur. J.* **1998**, *4*, 118–126.
12. Feng, Y.; Li, J.; Jiang, L.; Gao, Z.; Huang, W.; Jiang, F.; Luo, N.; Han, S.; Zeng, R.; Yang, D. *Eur. J. Org. Chem.* **2011**, 562–568.
13. (a) Saha, A.; Ramakrishnan, S. *Macromolecules* **2009**, *42*, 4028–4037; (b) Malashikhin, S.; Finney, N. S. *J. Am. Chem. Soc.* **2008**, *130*, 12846–12847.
14. Senthilvelan, A.; Ho, I.; Chang, K.; Lee, G.; Liu, Y.; Chung, W. *Chem.—Eur. J.* **2009**, *15*, 6152–6160.
15. (a) Benesi, H. A.; Hildebrand, J. H. *J. Am. Chem. Soc.* **1949**, *71*, 2703–2707; (b) Singh, R. B.; Mahanta, S.; Guchhait, N. *J. Mol. Struct.* **2010**, *963*, 92–97.